Design and Test of Crab-Shaped Negative Group Delay Circuit

Blaise Ravelo, Fayu Wan, Sebastien Lallechere, Glauco Fontgalland, Wenceslas Rahajandraibe

Design and Test of Crab-Shape Negative Group Delay Circuit

Blaise Ravelo, *Member*, *IEEE*, Fayu Wan, *Member*, *IEEE*, Sébastien Lalléchère, *Member*, *IEEE*, Glauco Fontgalland, *Senior Member*, *IEEE* and Wenceslas Rahajandraibe, *Member*, *IEEE*

***Abstract*—This paper presents the design and test of a distributed planar microwave circuit presenting a crab-shape topology. The circuit's topology consists of transmission lines (TLs) associated in feedback with two cascaded coupled lines (CLs). This topology has the characteristics of a bandpass negative group delay (NGD) function. The analytical model allowing to determine the group delay (GD) is established from S-parameter approach and the analysis of NGD crab topology is described. The NGD existence condition as a function of the topological parameters is presented. The NGD circuit proof-of-concept (PoC) is designed, simulated, and fabricated to understand and validate the proposed NGD functions. The measured, simulated, and theoretical results are in good agreement. As designed, the band pass NGD behavior is observed around 3 GHz with NGD of approximately -4.8 ns.**

***Index Terms*— Coupled lines (CLs), Distributed circuit modelling, crab-shape topology, bandpass negative group delay (NGD), microwave circuit.**

I. Introduction

THE MICROWAVE SIGNAL DELAYS can be one of challenging issues, which may influence the performances of modern communication systems. The technical solutions introduced to overcome this issue apply all pass networks with group delay (GD) slope control, allowing enhancement of analog signal processing resolution [1-2]. Most of those all pass network control techniques are usually complex and insufficient against the GD effects [3].

A particularly emerging equalization technique based on the negative group delay (NGD) function has been initiated since more than a dozen year [4-6]. This uncommon delay reduction technique consists of neutralizing the positive GD by the culprit circuit with an NGD function. The NGD equalization technique enables also to neutralize the RC- and LC-interconnect effects encountered regularly by signal integrity (SI) engineers [6]. In addition to the delay issue, the NGD function was also used to improve RF and microwave devices performance, such as the feedforward amplifier linearization [7], antenna array by eliminating the beam squint [8], and also design a challenging device as non-Foster reactive elements [9-10].

Despite the progressive research interests, the NGD function remains unfamiliar to most of electronic and signal integrity engineers. Therefore, it is worth describing more in details the state of the art on the NGD topic. The NGD function was initially experimented in the microwave frequencies with literally complex and extremely lossy circuits [11-15]. The NGD function was investigated with typically microwave circuits built with typically resonant RLC-networks [11-12,15]. Then, the NGD function was reinitiated with metamaterial microwave circuit revolution with the negative refractive index (NRI) transmission lines (TLs) [13-14]. In term of design process, series and parallel RLC resonant networks are basic and commonly NGD circuit units. Because of excessive losses, less research interests have been conducted on the NGD topic last in the middle of 2000s. The lumped component based NGD passive circuits designed in 2000s present tremendous limitations because of the attenuation, design complexity and frequency bandwidth limitations.

To further understand the basic NGD properties of NGD function, its similarity with the classical filter function behaviors was stated [16]. A synthesis methodology of all pass band NGD cell was introduced in [17]. More research works regarding the bandpass NGD microwave circuits design have been published by different worldwide groups in 2010s [16-27]. The results of these recent NGD investigations clarify usually the doubts about the intriguing NGD phenomenon existence. Most of NGD circuit design methods [18-29] were aimed to identify the NGD center frequency, by size's reduction and, especially, to solve the challenge of NGD transmission coefficient attenuation reduction lower than 10 dB. The design feasibility of NGD distributed microwave circuit that may not need lumped circuits was confirmed [18-19,25,32,33]. Further challenge related to the compact NGD circuit design was also

Manuscript received xxx xx, 2020; revised xxx xx, 2020; accepted xxx xx, 2020. Date of publication xxx xx, 2020.

This research work was supported in part by NSFC under Grant 61601233 and Grant 61750110535, in part by NSF of Jiangsu under Grant BK20150918, in part by the Jiangsu Innovation and Enterprise Group Talents Plan 2015 under Grant SRCB201526, and in part by PAPD.

Blaise Ravelo, and Fayu Wan are with the Nanjing University of Information Science & Technology (NUIST), Nanjing 210044, Jiangsu, China (e-mail: blaise.ravelo@nuist.edu.cn, Corresponding author e-mail: fayu.wan@nuist.edu.cn).

Sébastien Lalléchère is with the Université Clermont Auvergne (UCA), CNRS, SIGMA Clermont, Institut Pascal, Aubière, France. (email: sebastien.lallechere@uca.fr).

Glauco Fontgalland is with Federal University of Campina Grande, Applied Electromagnetic and Microwave Lab., Campina Grande/PB, 58429, Brazil. (email: fontgalland@dee.ufcg.edu.br).

Wenceslas Rahajandraibe is with the Aix-Marseille University, CNRS, University of Toulon, IM2NP UMR7334, Marseille, France (E-mail: wenceslas.rahajandraibe@im2np.fr).

made in [22,24,26]. In term of implementation, one of the most performing distributed NGD circuit designs are based on the use of TLs and coupled lines (CLs) [19,22]. Some of TL NGD networks can be typically accomplished by using TL stubs with loaded resistors. By using a distributed TL, a novel design method of the filter based on the NGD circuit is reported [21] and the GD can be perfectly controlled by the resistors.

This innovative idea is deeply investigated in the present paper by considering the distributed topology of "crab"-shape geometry structure. The proposed topology of microwave circuit is susceptible to operate as a bandpass NGD microwave circuit. The proposed NGD topology consists of two identical CLs and a feedback TL. The total GD can be simultaneously controlled via the coupling coefficients and TL electrical length.

The paper is divided into three main sections. Section II deals with the NGD theory of crab-shape topology. In this section, the S-parameter and GD modelling is developed and thus the NGD analysis will be presented based on the transmission coefficient exploitation. Section III will be focused on simulation and experimental validations. The effect of the proposed crab-shape topology key parameters on the NGD performance will be evaluated. Simulated and measured results from a proof-of-concept (PoC) will be discussed. Finally, Section IV concludes the paper.

II. NGD Design Concept of the Crab-Shape Topology

This section describes the NGD theory of crab-shape inspired topology. The equivalent S-parameter model is derived and the GD analysis is established in order to confirm the multi-band and bandpass NGD function.

A. Topological Description

Fig. 1 depicts the topology of the crab-shape NGD circuit, which is assumed as a two-port network. It acts as a fully distributed topology built without using lossy lumped elements. The topology consists of CLs named CL_1 and CL_2 whose direct ports and coupled ports are connected by TLs TL_1 and TL_2, respectively. The CL isolated ports are open-circuited. The TLs are supposed ideally matched with a characteristic impedance R_0=50 Ω. TL_1 is necessary to avoid the electrical contact and to control the coupling between the open-ended terminal of the CLs. TL_1 electrical effect is supposed negligible.

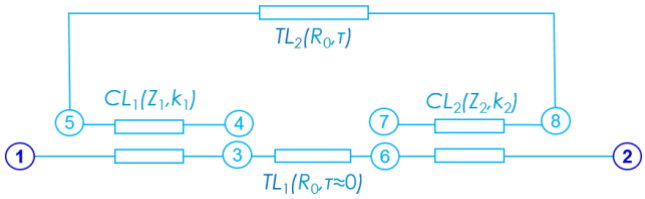

Fig. 1. Configuration of the crab-shape inspired topology.

TL_2 is defined with physical length d, electrical length θ, and time delay τ linked by the relationships:

$$\begin{cases} \tau = \dfrac{d}{v} \\ \theta(\omega) = \omega\tau \end{cases}, \tag{1}$$

where v is the signal wave speed and ω is the angular frequency variable.

B. Analysis of the Coupled TLs Constituting the Proposed Circuit Topology

Based on the previous paragraph assumption, the proposed topology can be represented by the two-port block diagram sketched in Fig. 2. Before elaborating the global S-parameter model, it is worth to remind the elementary TL and CL theory.

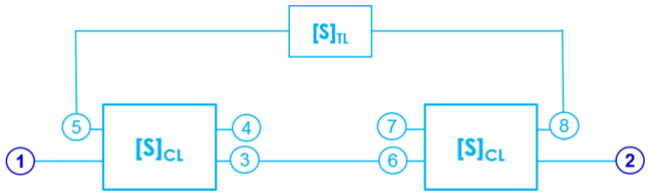

Fig. 2. Equivalent diagram of the topology introduced in Fig. 1.

1) Recall on TL Coupled Line Theory

Assigned as perfectly matched, the feedback lossy TL S-parameter can be written as:

$$\left[S(j\omega)\right]_{TL} = \begin{bmatrix} S_{11}(j\omega) & S_{21}(j\omega) \\ S_{21}(j\omega) & S_{11}(j\omega) \end{bmatrix} = \begin{bmatrix} 0 & a\cdot e^{-j\omega\tau} \\ a\cdot e^{-j\omega\tau} & 0 \end{bmatrix}, \tag{2}$$

by denoting a as frequency independent TL loss. CL_1 and CL_2 are identical and defined by the coupling coefficient k whose even- and odd-mode impedances are

$$\begin{cases} Z_e = R_0\sqrt{\dfrac{1+k}{1-k}} \\ Z_o = R_0\sqrt{\dfrac{1-k}{1+k}} \end{cases} \tag{3}$$

where

$$Z_e Z_o = R_0^2 . \tag{4}$$

For the sake of the analytical simplification, the coupled lines are supposed to be no-delayed and have the access ports ideally matched to R_0. The CL four-port block S-parameter is given as

$$\left[S\right]_{CL} = \begin{bmatrix} 0 & k_1 & 0 & k \\ k_1 & 0 & k & 0 \\ 0 & k & 0 & k_1 \\ k & 0 & k_1 & 0 \end{bmatrix} \tag{5}$$

where

$$k_1 = -j\,k_0 = -j\sqrt{1-k^2}\,, \tag{6}$$

and j^2=-1. Based on these quantities, the NGD topology S-parameter is established in the following paragraph.

C. S-Parameter Modelling of the Proposed Topology

The global S-parameter of the circuit diagram introduced in Fig. 2 is established by considering the power waves a_m and b_m (m={1,2,…,8}) by referring to the four-port blocks of CL_1 and CL_2. With the assigned characteristics of TL_1 defined in the previous paragraph, we have

$$\begin{cases} b_3 = a_6 \\ a_3 = b_6 \end{cases} \tag{7}$$

and for TL_2, the relationship for a_5, a_8, b_5, and b_8 power waves can be written as

$$\begin{cases} a_5 = a \cdot e^{-j\omega\tau} \times b_8 \\ a_8 = a \cdot e^{-j\omega\tau} \times b_5 \end{cases}. \quad (8)$$

Following the port numbers, we have the S-matrix relationships:

$$\begin{cases} \begin{bmatrix} b_1 \\ b_3 \\ b_4 \\ b_5 \end{bmatrix} = [S]_{CL} \begin{bmatrix} a_1 \\ a_3 \\ a_4 \\ a_5 \end{bmatrix} \\ \begin{bmatrix} b_2 \\ b_6 \\ b_7 \\ b_8 \end{bmatrix} = [S]_{CL} \begin{bmatrix} a_2 \\ a_6 \\ a_7 \\ a_8 \end{bmatrix} \end{cases}. \quad (9)$$

After solving the overall equation system combining (7), (8) and (9), the following, respectively, reflection and transmission coefficients are established:

$$S_{11}(j\omega) = \frac{k^2 k_0^2 (1 + a\, e^{-j\omega\tau})^2}{(k_0^2 a\, e^{-j\omega\tau} - k^2)^2 - 1}, \quad (10)$$

$$S_{21}(j\omega) = \frac{\left[k_0 a\, e^{-j\omega\tau}(k^2 + k_0^2)\right]^2 - k^2 a\, e^{-j\omega\tau}\left[(k^2 + k_0^2)^2 - 1\right] - k_0^2}{(k_0^2 a\, e^{-j\omega\tau} - k^2)^2 - 1}. \quad (11)$$

The associated magnitudes are given by

$$S_{11}(\omega) = |S_{11}(j\omega)| = \frac{k^2 \sqrt{\left[a + \cos(\tau\omega)\right]^2 + \sin^2(\tau\omega)}}{\sqrt{\left[a(k^2 - 1) + (k^2 + 1)\cos(\tau\omega)\right]^2 + (k^2 + 1)^2 \sin^2(\tau\omega)}}, \quad (12)$$

$$S_{21}(\omega) = |S_{21}(j\omega)| = \frac{\sqrt{\left[a - \cos(\tau\omega)\right]^2 + \sin^2(\tau\omega)}}{\sqrt{\left[a(k^2 - 1) + (k^2 + 1)\cos(\tau\omega)\right]^2 + (k^2 + 1)^2 \sin^2(\tau\omega)}}. \quad (13)$$

The transmission phase is expressed as:

$$\varphi(\omega) = \varphi_n(\omega) - \varphi_d(\omega), \quad (14)$$

with

$$\varphi_n(\omega) = \arctan\left[\frac{\sin(\tau\omega)}{\cos(\tau\omega) - a}\right] \quad (15)$$

and

$$\varphi_d(\omega) = \arctan\left[\frac{(k^2 + 1)\sin(\tau\omega)}{a(k^2 - 1) + (k^2 + 1)\cos(\tau\omega)}\right]. \quad (16)$$

D. NGD Analysis

The GD is defined from the transmission coefficient by the relation:

$$\tau_t(\omega) = \frac{-\partial\varphi(\omega)}{\partial\omega}. \quad (17)$$

By applying this definition to the transmission phase written in (14), the following expression is established:

$$\tau_t(\omega) = \tau_d(\omega) - \tau_n(\omega), \quad (18)$$

with

$$\tau_n(\omega) = \frac{\tau\left[1 - a\cos(\tau\omega)\right]}{1 + a^2 - 2a\cos(\tau\omega)}, \quad (19)$$

$$\tau_d(\omega) = \frac{\tau(k^2 + 1)\left[k^2 + 1 + a(k^2 - 1)\cos(\tau\omega)\right]}{\left[(k^2 - 1)\left[2a(k^2 + 1)\cos(\tau\omega) + a^2(k^2 - 1)\right] + (k^2 + 1)^2\right]} \quad (20)$$

The NGD existence condition can be derived from expression (18), which is determined by inequation:

$$\tau_t(\omega) < 0. \quad (21)$$

Therefore, we have the following conditions:

$$\begin{cases} \alpha_1 \cos(\tau\omega) + \alpha_0 > 0 \\ \alpha_3 \cos(\tau\omega) + \alpha_2 < 0 \end{cases}, \quad (22)$$

or

$$\begin{cases} \alpha_1 \cos(\tau\omega) + \alpha_0 < 0 \\ \alpha_3 \cos(\tau\omega) + \alpha_2 > 0 \end{cases}, \quad (23)$$

with:

$$\begin{cases} \alpha_0 = 2a \\ \alpha_1 = a^2(k^2 - 1) - 1 - k^2 \\ \alpha_2 = a^2(1 - k^2)^2 + (1 + k^2)^2 \\ \alpha_3 = 2(k^4 - 1) \end{cases}. \quad (24)$$

E. NGD Characterization Around Particular Frequencies

The NGD characterization can be focused on a family of trivial angular frequency given by

$$\omega_m = \frac{2\pi m}{\tau}, \quad (25)$$

with m={0,1,2,3,…}. The simplified expressions of reflection and transmission coefficients derived from equations (12) and (13) can be expressed as

$$S_{11}(\omega_m) = \frac{k^2(1 + a)}{k^2(1 + a) + 1 - a}, \quad (26)$$

$$S_{21}(\omega_m) = \frac{1 - a}{k^2(1 + a) + 1 - a}. \quad (27)$$

At the same frequency, the GD introduced in equation (18) is simplified as

$$\tau_m = \tau(\omega_m) = \frac{-2k^2 a\, \tau}{(1 - a)\left[k^2(1 + a) + 1 - a\right]}. \quad (28)$$

As a<1, this GD is always negative for any values of the proposed topology parameters. This finding means that because the frequency-dependent S-parameter periodicity, this passive topology can behave at the same time as a low pass, a bandpass, and multiband NGD function. Moreover, the NGD cut-off frequencies $\omega = \omega_c$ can be determined as the roots of equation

$$\tau_t(\omega) = 0. \quad (29)$$

By considering equation (16), with the relative integer m={0,1,2,…}, the cut-off frequencies are given by

$$\omega_{c_1}(m) = \frac{\arccos\left[\frac{2a}{1 + k^2 + a^2(1 - k^2)}\right] + 2\pi m}{\tau}, \quad (30)$$

$$\omega_{c_2}(m \geq 1) = \frac{2\pi m - \arccos\left[\frac{2a}{1+k^2+a^2(1-k^2)}\right]}{\tau}. \quad (31)$$

As reported in [16-17], in low pass function, the NGD bandwidth is equal to the cut-off frequency

$$\Delta\omega_{low\,pass} = \omega_c(0). \quad (32)$$

For m>0, the bandpass NGD bandwidth around the NGD center frequencies ω_m expressed in (25), is defined by the difference between the successive cut-off frequencies:

$$\Delta\omega_{bandpass}(m) = \omega_{c_2}(m) - \omega_{c_1}(m). \quad (33)$$

Based on the similitude between the filter and NGD theory [16-17], we remind that the generalized bandpass NGD bandwidth is twice the low pass one:

$$\Delta\omega_{bandpass}(m) = 2\Delta\omega_{low\,pass}. \quad (34)$$

Consequently, for m={1,2,3,…}, the formula of the generalized bandpass NGD bandwidth can be written as

$$\Delta\omega_{bandpass}(m) = 2\arccos\left[\frac{2a}{1+k^2+a^2(1-k^2)}\right]. \quad (35)$$

F. Design Methodology of Crab-Shape NGD Circuit

The general process to design the crab-shape NGD circuit must begin with the expected fabrication technology and the targeted NGD specifications as desired value of NGD at the center frequency. Then, we can follow the design guideline indicated in the following three successive phases:

- ***Phase 1***: At the beginning of the design process, the NGD function operating around the expected centre frequency must be specified. Then, the analytical computation can be realized based on the ideal model of the S-parameters. Parametric analyses in function of NGDC parameters can also be performed. This analysis allows a better comprehension of influence of parameters on the NGD performance.
- ***Phase 2***: In this intermediate phase, the NGD design engineer must take care on the available technology for fabricating the NGD prototype. For example, in the present study, as it will be explored in the next validation section, we will deal with microstrip technology to design and to implement our NGD prototype. Therefore, in this phase, the NGDC can be designed and simulated with the commercial tools (as the RF and microwave circuit ADS® designer and simulator from Keysight Technologies® or HFSS® from ANSYS®). The circuit simulations of the present phase should include the NGD prototype realistic effects. For example, the extra interconnect lines as the input/output access lines, the electrical interconnects and also the substrate material parameters provided by the manufacturer must be considered before the PCB 3-D layout design. Then, probable optimizations taking into account the realistic effects as the TL widths and lengths can be necessary.
- ***Phase 3***: In this last phase, the NGD prototype must be fabricated from the PCB layout drawn from the optimized design performed in Phase 2. Acting as an RF and microwave circuit, the NGD prototype can be tested with a Vector Network Analyzer (VNA). Before the tests, the VNA must be calibrated with consideration of the working frequency. The NGD test must start with the S-parameter measurements.

The basic steps of NGDC design and test are summarized in the workflow of Fig. 3.

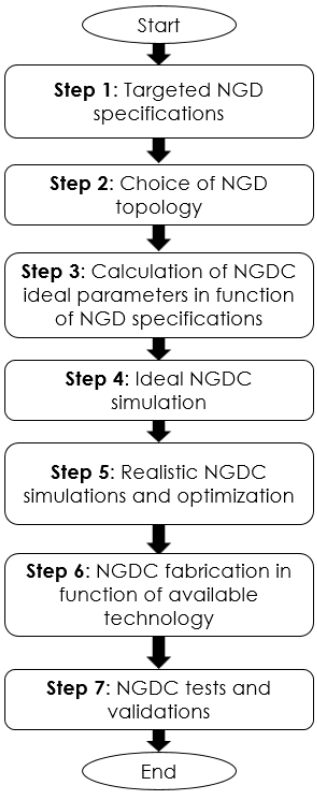

Fig. 3. Workflow of NGDC design and test method.

To materialize the feasibility of the developed NGD theory, PoC practical investigation will be presented in the next section.

III. PRACTICAL VALIDATIONS

The present section deals with the validations of the crab-shape NGD topology. After the PoC description, parametric simulations are described in order to quantify the effects of CL coupling space, whole circuit width and feedback TL_2 length. The overall validation aspects are originally focused on analyzing NGD function.

A. PoC Design Description

The NGD prototype was implemented on Cu-metalized Rogers 3210 dielectric substrate in microstrip technology without lossy lumped component. The substrate physical characteristics are addressed in Table I. After parameters design optimization, the microstrip prototype introduced in Figs. 4 was designed and fabricated. The optimized geometrical and electrical parameters of this prototype are indicated in Table I. The microstrip circuit layout shown in Fig. 4(a) was designed in the HFSS® environment. The fabricated prototype which presents the physical sizes 21 mm × 41 mm, is showed in Fig. 4(b).

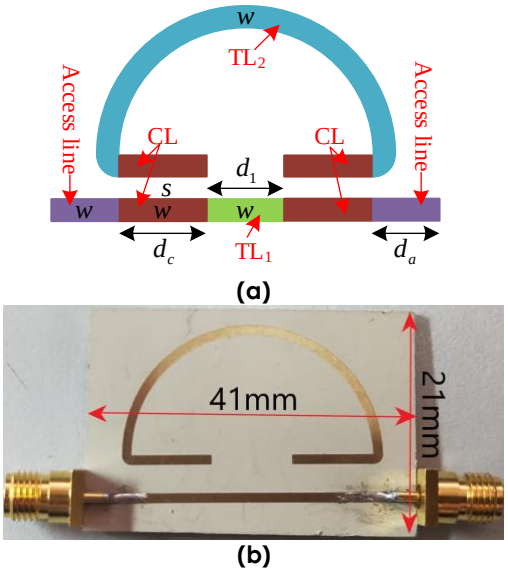

Fig. 4. (a) Layout and (b) photograph of the NGD prototype.

TABLE I
PHYSICAL PARAMETER DIMENSIONS OF THE NGD PROTOTYPE

Structure	Description	Parameters	Values
Substrate	Relative permittivity	ε_r	10.2
	Loss tangent	tan(δ)	0.0027
	Thickness	h	1.27 mm
Metallization conductor	Copper conductivity	σ	58 MS/s
	Thickness	t	35 µm
CL	Space	s	3.5 mm
	Width	w	1.184 mm
	Length	d_c	10.44 mm
	Coupling coefficient	k	-26 dB
	Even- and odd-mode characteristic impedance	Z_e	49 Ω
		Z_o	45 Ω
Feedback TL_2	width	w	1.184 mm
	Time-delay	τ	0.32 ns
	Attenuation	a	-0.15 dB
	Overall length	d_2	53.23 mm
TL_1	Length	d_1	10.44 mm
	width	w	1.184 mm
Access line	Length	d_a	5 mm
	width	w	1.184 mm

B. *Parametric Analyses*

Parametric analyses with respect to the feedback TL delay τ and CL coupling coefficient k have been conducted. The parametric analyses enable to explain more explicitly the feedback TL and CL effects onto the NGD function. Simulations from 1.6 GHz to 3 GHz are carried out with the ADS® electronic and RF/microwave simulation tools from Keysight technologies®. During the simulations, the TL loss was fixed to a=-0.95 dB.

1) *Parametric Analysis Versus the CL Coupling Coefficient*

The CL effect was investigated by varying coupling coefficient k from -15 dB to -10 dB with τ fixed to 0.62 ns during the S-parameter simulations. Figs. 5 displays the cartographies of the obtained GD and S_{21} versus (f,k). As depicted in Fig. 5(a), two NGD center frequencies appeared around f_1=1.61 GHz and f_2=3.22 GHz insensitively to the variation of k. Fig. 6 and Fig. 7 show the zoom in of GD around the center frequencies.

Within the considered variation range, the absolute value of NGD level is decreasing when k decreases. Moreover, S_{21} behavior is similar to the GD. In the considered range of k, S_{21} varies between -3 dB and -8 dB. To validate the expressions of $\tau_t(f_1,f_2)$, $S_{21}(f_1,f_2)$, and $\Delta\omega_{1,2}$ formulated in (27), (28) and (35), respectively, Table II addresses comparisons between calculations and ADS® schematic S-parameter simulations for k={-15 dB, -13 dB, -11 dB, -10 dB}. As expected, the calculations are in good agreement with simulations.

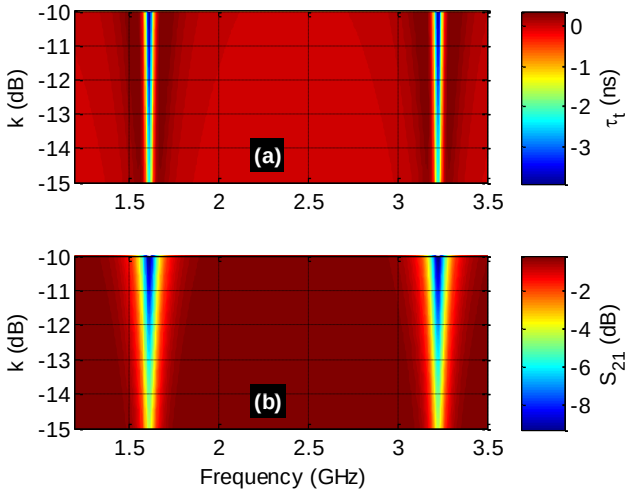

Fig. 5. Parametric results versus k: (a) GD and (b) S_{21}.

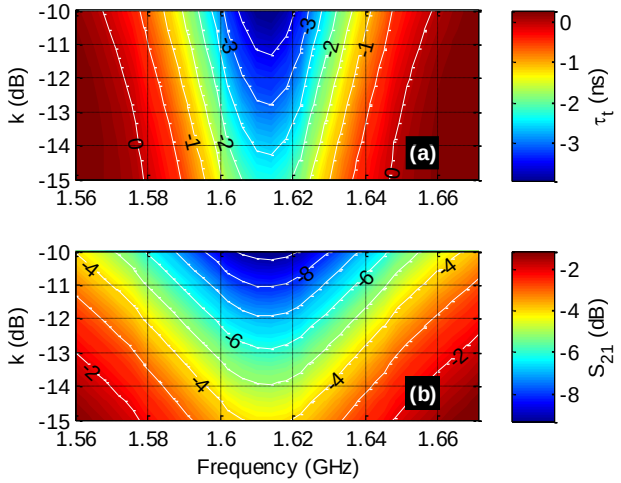

Fig. 6. Zoom in of (a) GD and (b) S_{21} versus k around f_1.

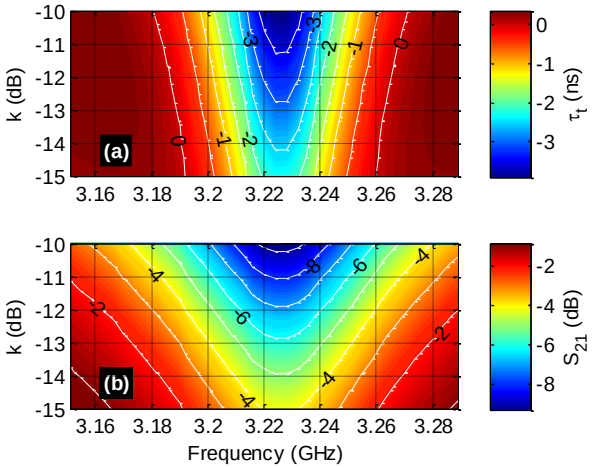

Fig. 7. Zoom in of (a) GD and (b) S_{21} versus k around f_2.

TABLE II
COMPARISON OF SIMULATED AND CALCULATED IDEAL CIRCUIT PARAMETERS VERSUS K

Approach	k (dB)	$\tau_t(f_1)$ (ns)	$S_{21}(f_1)$ (dB)	$\Delta\omega_1$ (MHz)
Simulation	-15	-2.265	-4.142	67
	-13	-2.938	-5.882	74
	-11	-3.616	-8.078	84
	-10	-3.935	-9.343	90
Calculation	-15	-2.265	-4.137	67
	-13	-2.938	-5.881	74
	-11	-3.616	-8.072	84
	-10	-3.935	-9.343	90
Approach	**k (dB)**	**$\tau_t(f_2)$ (ns)**	**$S_{21}(f_2)$ (dB)**	**$\Delta\omega_2$ (MHz)**
Simulation	-15	-2.265	-4.142	67
	-13	-2.938	-5.882	74
	-11	-3.616	-8.078	84
	-10	-3.935	-9.343	90
Calculation	-15	-2.265	-4.141	67
	-13	-2.938	-5.876	74
	-11	-3.616	-8.078	84
	-10	-3.935	-9.343	90

2) Parametric Analysis Versus the Feedback TL Delay τ

Figs. 8 display the parametric simulation results versus the variation of feedback TL delay τ varied from 0.55 ns to 0.65 ns with k fixed to -14 dB. Once again, the NGD dual band behavior is obtained.

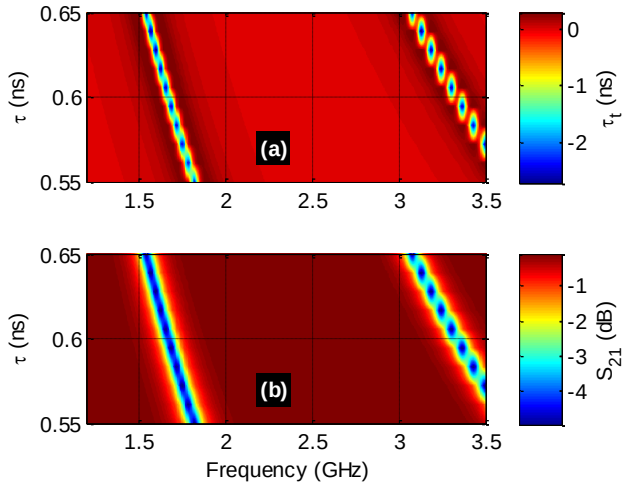

Fig. 8. Parametric results versus τ: (a) GD and (b) S_{21}.

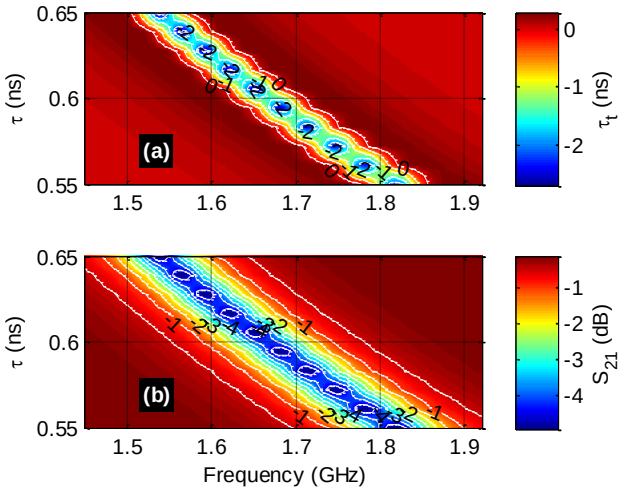

Fig. 9. Zoom in of (a) GD and (b) S_{21} versus τ around f_1.

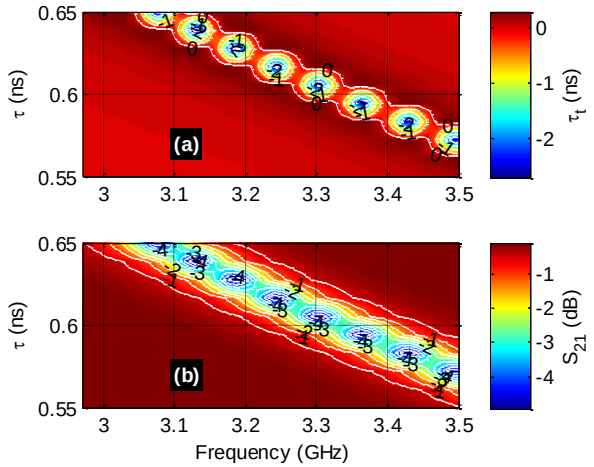

Fig. 10. Zoom in of (a) GD and (b) S_{21} versus τ around f_2.

TABLE III
COMPARISON OF SIMULATED AND CALCULATED IDEAL CIRCUIT PARAMETERS VERSUS τ

Approach	τ (ns)	f_1 (GHz)	$\tau_t(f_1)$ (ns)	$S_{21}(f_1)$ (dB)
Calculation	0.55	1.812	-2	-4.14
	0.6	1.666	-2.19	-4.14
	0.65	1.538	-2.37	-4.14
Simulation	0.55	1.819	-2.3	-4.9
	0.6	1.667	-2.51	-4.95
	0.65	1.538	-2.72	-4.95
Approach	**τ (ns)**	**f_2 (GHz)**	**$\tau_t(f_2)$ (ns)**	**$S_{21}(f_2)$ (dB)**
Calculation	0.55	3.636	-2	-4.14
	0.6	3.333	-2.19	-4.14
	0.65	3.076	-2.37	-4.14
Simulation	0.55	3.637	-2.3	-4.9
	0.6	3.333	-2.51	-4.95
	0.65	3.077	-2.72	-4.95

However, as shown in Fig. 9(a) and Fig. 10(a), the NGD center frequencies are decreasing when τ is increasing as predicted in formula (25). The GD level expressed in (27) is insensitive to the feedback delay variation. With the considered range of τ, S_{21} changes between -5 dB and -1 dB.

The expressions of $f_{1,2}$, $\tau_t(f_{1,2})$, and $S_{21}(f_{1,2})$ formulated in (25), (27), and (28) are validated with the results monitored in Table III. The calculations are well-correlated with ADS®

schematic S-parameter simulations for τ={0.55 ns, 0.6 ns, 0.65 ns}.

C. NGD Design Validation Results

The experimental validation of the proposed crab-shape NGD topology is explored in the present subsection. Comparisons of results obtained from calculations, HFSS® simulation using ANSYS®, and measurements are discussed.

1) Experimental Setup Configuration

Similar to classical microwave circuits, the NGD tests, which are based on S-parameter analysis, were performed with a Vector Network Analyzer (VNA). The fabricated NGD prototype, previously introduced in Fig. 4(b), was measured with VNA (Rohde & Schwarz ZNB 20, withing the frequency band 100 kHz to 20 GHz). The experimental setup can be seen in Fig. 11. The test was made under SOLT calibration.

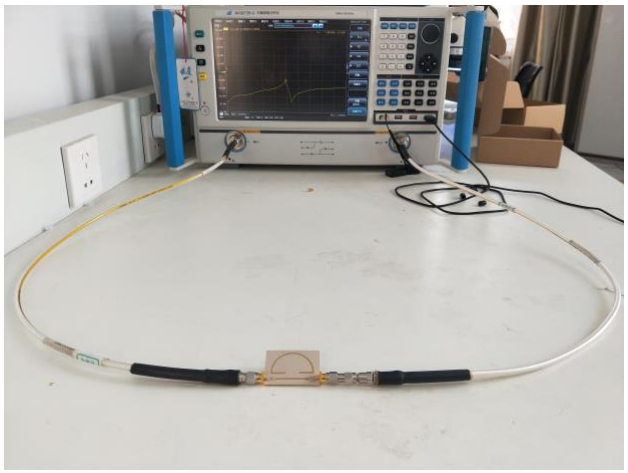

Fig. 11. Configuration of the crab-shape prototype experimental setup.

2) Discussion on Calculated, Simulated, and Tested Results

Comparisons between the calculated ("Calc."), simulated ("Sim.") with HFSS®, and measured ("Meas.") results have been carried out in the frequency band from 3 GHz to 3.2 GHz. The calculated results were obtained with a program developed in MATLAB using S-parameters equations introduced in (9), (10) and (16). The calculated, simulated, and measured GDs and S-parameters are plotted in Figs. 12. It can be pointed out that these comparative results present a very good agreement. As expected, in the working frequency band, the tested prototype behaves as a bandpass NGD behaviors around center frequency of approximately f_0=3.096 GHz. Table IV summarizes the differences between the calculated, simulated and measured NGD parameters. Figs. 12 illustrates the good performances of the crab NGD topology in terms of group delay, insertion and reflection losses at f_0. As depicted in Fig. 12(a), the tested crab-shape circuit has NGD of approximately -4.8 ns over 15 MHz bandwidth. The slight frequency shifts of NGD center frequency are mainly due to the fabrication inaccuracies, substrate effective permittivity tolerance, and losses versus the numerical computation accuracy. It can be seen from Fig. 12(b) and 12(c) that in the test frequency band, S_{21} and S_{11} are globally better than -3 dB and -11 dB, respectively.

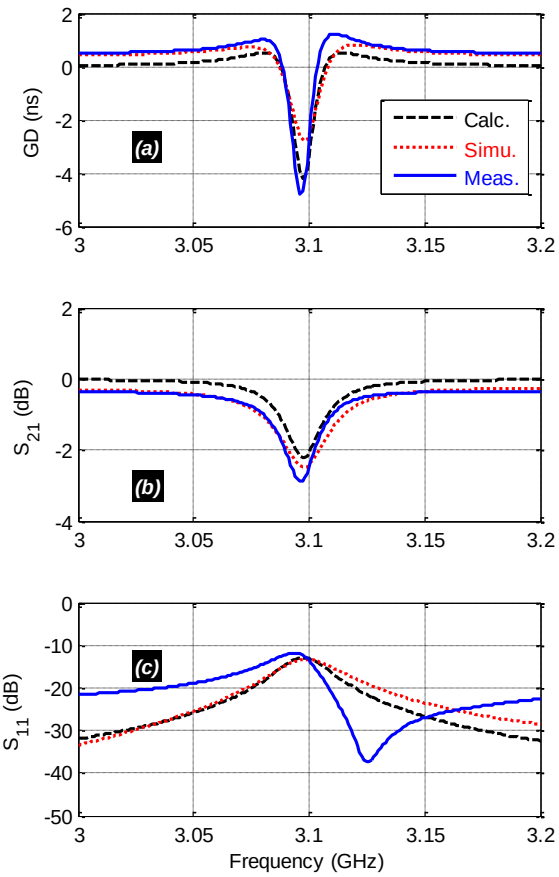

Fig. 12. Comparisons of calculated, measured, and simulated (a) GD and (b) transmission parameters from the crab-shape prototype shown in Fig. 4(b).

TABLE IV
COMPARISON OF SIMULATED AND MEASURED NGD PROTOTYPE PARAMETERS

Validation method	f_o (GHz)	$\tau(f_o)$ (ns)	*BW* (MHz)	$S_{21}(f_o)$ (dB)	$S_{11}(f_o)$ (dB)
Calc.	3.098	-4.2	19	-2.21	-12.95
Simu.	3.098	-2.8	21	-2.48	-13.32
Meas.	3.096	-4.8	15	-2.87	-11.83

D. NGD Comparative Study

Table V introduces the comparisons on S-parameters and NGD between the proposed crab-shape topology and the other ones published in literature [19, 23, 26, 26-29]. This comparison considers the NGD figure of merit (FoM) defined as [23]

$$FoM = BW_{NGD}\left|S_{21}(jf_0)\right|\left|\tau(f_0)\right|. \quad (36)$$

TABLE V
COMPARISON OF NGD SPECIFICATIONS

Ref.	**f_0 (GHz)**	**$\tau(f_o)$ (ns)**	**$S_{21}(f_o)$ (dB)**	**$S_{11}(f_o)$ (dB)**	**FoM**	**Use of lossy resistor**
[19]	1.26	-2.2	-2.4	-13	0.0334	No
[23]	1.01	-2.09	-18.1	-33	0.0375	Yes
[26]	1.79	-7.7	-8.6	-20	0.1001	Yes
This work	3.096	-4.8	-2.87	-11.83	0.0517	No

It is worth emphasizing that the crab NGD circuit exhibits the following advantages on design simplicity, considerable fully distributed elements without lossy lumped component, low attenuation loss less than 3 dB, high NGD values, larger than -4 ns and the possibility to operate up to several GHz. The NGDC proposed in the present work has a better overall performance including FoM and loss compared to most of existing ones. The NGDC designed in [26] presents a good FoM but has a significant loss.

IV. Conclusion

A novel NGD circuit inspired from the crab-shape topology is investigated. The proposed topology consists of CLs and TL, assumed with same characteristic impedances. The S-parameter model is established for the NGD analysis. Different particular frequencies related to the TL length are identified.

To confirm the feasibility of the Crab-shape NGD theory, an NGD PoC has been designed and implemented. Parametric analyses with respect to the NGD prototype key parameters are performed. It was emphasized that the NGD performance depends tightly on the CL coupling coefficient and also the TL physical length. Moreover, experimental studies were also carried out. The fabricated NGD circuit prototype showed a very good agreement between simulation and measurement.

References

[1] S. Gupta, A. Parsa, E. Perret, R.V. Snyder, R.J. Wenzel and C. Caloz, "Group-Delay Engineered Noncommensurate Transmission Line All-Pass Network for Analog Signal Processing," IEEE Trans. Microwave Theory Techn., vol. 58, no. 9, Dec. 2010, pp. 2392-2407.

[2] B. Nikfal, S. Gupta and C. Caloz, "Increased Group-Delay Slope Loop System for Enhanced-Resolution Analog Signal Processing," IEEE Trans. Trans. Microwave Theory Techn., vol. 59, no. 6, June 2011, pp. 1622-1628.

[3] S.-S. Myoung, B.-S. Kwon, Y.-H. Kim and J.-G. Yook, "Effect of group delay in RF BPF on impulse radio systems," IEICE Trans. on Communications, vol. 90, no. 12, pp. 3514-3522, 2007.

[4] K.-P. Ahn, R. Ishikawa, and K. Honjo, "Group delay equalized UWB InGaP/GaAs HBT MMIC amplifier using negative group delay circuits," IEEE Trans. Microwave Theory Techn., vol. 57, no. 9, pp. 2139- 2147, Sept. 2009.

[5] S. K. Podilchak, B. M. Frank, A. P. Freundorfer and Y. M. M. Antar, "High Speed Metamaterial-Inspired Negative Group-delay Circuits in CMOS for Delay Equalization," in Proc. of 2nd Microsystems and Nanoelectronics Research Conference 2009 (MNRC 2009), Ottawa, ON, 13-14 Oct. 2009, pp. 9-12.

[6] B. Ravelo, "Neutralization of LC- and RC-Effects with Left-Handed and NGD Circuits," Advanced Electromagnetics, vol. 2, no. 1, Sept. 2013, pp. 73-84.

[7] H. Choi, G. Chaudhary, T. Moon, Y. Jeong, J. Lim, and C. D. Kim, "A design of composite negative group delay circuit with lower signal attenuation for performance improvement of power amplifier linearization techniques," IEEE MTT-S Int. Microw. Symp. Dig., Jun. 2011, pp. 1-4.

[8] W. Alomar and A. Mortazawi, "Elimination of beam squint in uniformly excited serially fed antenna arrays using negative group delay circuits," in Proc. IEEE Int. Symp. Antennas Propag., Chicago, IL, USA, Jul. 2012, pp. 1-2.

[9] H. Mirzaei and G. V. Eleftheriades, "Realizing non-Foster reactive elements using negative-group-delay networks," IEEE Trans. Microw. Theory Techn., vol. 61, no. 12, pp. 4322-4332, Dec. 2013.

[10] T. Zhang, R. Xu and C. M. Wu, "Unconditionally Stable Non-Foster Element Using Active Transversal-Filter-Based Negative Group Delay Circuit," IEEE Microw. Wireless Compon. Lett., vol. 27, no. 10, pp. 921-923, Oct. 2017.

[11] S. Lucyszyn and I. D. Robertson, "Analog reflection topology building blocks for adaptive microwave signal processing applications," IEEE Trans. Microw. Theory Techn., vol. 43, no. 3, pp. 601-611, Mar. 1995.

[12] S. Lucyszyn, I. D. Robertson, and A. H. Aghvami, "Negative Group Delay Synthesiser," Electron. Lett., vol. 29, no. 9, pp. 798-800, Apr. 1993.

[13] O. F. Siddiqui, M. Mojahedi and G. V. Eleftheriades, "Periodically Loaded Transmission Line with Effective Negative Refractive Index and Negative Group Velocity," IEEE Trans. Ant. Prop., vol. 51, no. 10, Oct. 2003, pp. 2619-2625.

[14] O. F. Siddiqui, S. J. Erickson, G. V. Eleftheriades, and M. Mojahedi, "Time-Domain Measurement of Negative-Index Transmission-Line Metamaterials," IEEE Trans. Microw. Theory Techn., vol. 52, no. 5, pp. 1449-1453, May 2004.

[15] F. Wan, N. Li, B. Ravelo, Q. Ji, B. Li and J. Ge, "The Design Method of the Active Negative Group Delay Circuits Based on a Microwave Amplifier and an RL-series Network," IEEE ACCESS, vol6, 2018, pp. 33849-33858.

[16] B. Ravelo, "Similitude between the NGD function and filter gain behaviours," Int. J. Circ. Theor. Appl., Vol. 42, No. 10, Oct. 2014, pp. 1016–1032.

[17] B. Ravelo, F. Wan and J. Feng, "All-Pass Negative Group Delay Function With Transmission Line Feedback Topology," IEEE Access, vol. 7, 2019, pp. 155711-155723.

[18] G. Chaudhary and Y. Jeong, "Distributed transmission line negative group delay circuit with improved signal attenuation," IEEE Microw. Wireless Compon. Lett., vol. 24, no. 1, pp. 20-22, Jan. 2014.

[19] B. Ravelo, "Theory of coupled line coupler-based negative group delay microwave circuit," IEEE Trans. Microw. Theory Techn., vol. 64, no. 11, pp. 3604-3611, Nov. 2016.

[20] G. Chaudhary and Y. Jeong, "A design of power divider with negative group delay characteristics," IEEE Microw. Wireless Compon. Lett., vol. 25, no. 6, pp. 394-396, Jun. 2015.

[21] L.-F. Qiu, L.-S. Wu, W.-Y. Yin, and J.-F. Mao, "Absorptive bandstop filter with prescribed negative group delay and bandwidth," IEEE Microw. Wireless Compon. Lett., vol. 27, no. 7, pp. 639-641, Jul. 2017.

[22] T. Shao, Z. Wang, S. Fang, H. Liu, and S. Fu, "A compact transmission line self-matched negative group delay microwave circuit," IEEE Access, vol. 5. pp. 22836-22843, Oct. 2017.

[23] Z. Wang, Y. Cao, T. Shao, S. Fang and Y. Liu, "A Negative Group Delay Microwave Circuit Based on Signal Interference Techniques," IEEE Microw. Wireless Compon. Lett., vol. 28, no. 4, pp. 290-292, Apr. 2018.

[24] T. Shao, S. Fang, Z. Wang and H. Liu, "A Compact Dual-Band Negative Group Delay Microwave Circuit," Radio Engineering, vol. 27, no.4, pp. 1070-1076, Dec. 2018.

[25] C.-T. M. Wu, S. Gharavi, B. Daneshrad, and T. Itoh, "A dual-purpose reconfigurable negative group delay circuit based on distributed amplifiers," IEEE Microw. Wireless Compon. Lett., vol. 23, no.11, pp. 593-595, Nov. 2013.

[26] G. Liu and J. Xu, "Compact transmission-type negative group delay circuit with low attenuation," Electron. Lett., vol. 53, no. 7, pp. 476-478, Mar. 2017.

[27] F. Wan, N. Li, B. Ravelo, Q. Ji, and J. Ge, "S-Parameter Model of Three Parallel Interconnect Lines Generating Negative Group-Delay Effect," IEEE Access, vol. 6, pp. 57152-57159, 2018.

[28] F. Wan, N. Li, B. Ravelo, and J. Ge, "O=O Shape Low-Loss Negative Group Delay Microstrip Circuit," IEEE Transactions on Circuits and Systems II, Access, 2019, pp. 1-5.

[29] F. Wan, Li. Wu, B. Ravelo, and J. Ge, "Analysis of Interconnect Line Coupled With a Radial-Stub Terminated Negative Group Delay Circuit," IEEE Trans. EMC, Early Access, 2019, pp.1-9.